



HAL
open science

Accelerated carbonation of recycled concrete aggregates: Investigation on the microstructure and transport properties at cement paste and mortar scales

Farah Kaddah, Harifidy Ranaivomanana, Ouali Amiri, Emmanuel Rozière

► To cite this version:

Farah Kaddah, Harifidy Ranaivomanana, Ouali Amiri, Emmanuel Rozière. Accelerated carbonation of recycled concrete aggregates: Investigation on the microstructure and transport properties at cement paste and mortar scales. *Journal of CO2 Utilization*, 2022, 57, pp.101885. 10.1016/j.jcou.2022.101885 . hal-04194697

HAL Id: hal-04194697

<https://hal.science/hal-04194697>

Submitted on 15 Nov 2023

HAL is a multi-disciplinary open access archive for the deposit and dissemination of scientific research documents, whether they are published or not. The documents may come from teaching and research institutions in France or abroad, or from public or private research centers.

L'archive ouverte pluridisciplinaire **HAL**, est destinée au dépôt et à la diffusion de documents scientifiques de niveau recherche, publiés ou non, émanant des établissements d'enseignement et de recherche français ou étrangers, des laboratoires publics ou privés.



Distributed under a Creative Commons Attribution - NonCommercial 4.0 International License

1 **Accelerated carbonation of recycled concrete aggregates:** 2 **investigation on the microstructure and transport** 3 **properties at the scale of cement paste and mortar.**

4 Farah Kaddah^a, Harifidy Ranaivomanana^b, Ouali Amiri^c, Emmanuel Rozière^{a,*}

5 Civil engineering and Mechanics Research Institute (GeM), UMR CNRS 6183,

6 ^a Ecole Centrale de Nantes, 1 rue de la Noe – 44321 Nantes, France

7 ^b IUT de Saint-Nazaire, 58 rue Michel Ange, 44606 Saint-Nazaire, France

8 ^c Polytech’Nantes, Campus Gavy, Boulevard de l’Université, 44603 Saint-Nazaire, France

9 * Corresponding author, Emmanuel.Roziere@ec-nantes.fr

10 **Abstract**

11 The accelerated carbonation of recycled concrete aggregates (RA) has been suggested to
12 improve their properties. Several physical and mechanical phenomena occur during the
13 carbonation of adhered cement mortar, but their effects are scarcely distinguished and
14 correlated. In this study cement paste and mortar specimens have been exposed to carbonation
15 after extended curing, and then characterized at different scales to monitor the evolution of
16 their microstructure and macroscopic properties as a function of their carbonation degree.
17 First the carbonation of portlandite and calcite precipitation dominate, then the carbonation of
18 C-S-H develops with the precipitation of vaterite and the development of material stiffness.
19 The increase in elastic modulus and carbonation shrinkage both favor microcracking: an
20 increase in macroporosity and permeability is actually observed. Clogging effect due to the
21 formation of calcium carbonate in the microstructure finally results in the reduction of the
22 porosity, pore sizes, and permeability.

23 **Keywords:** Cement, Carbonation, Recycled Concrete Aggregates, Hardness, Shrinkage,
24 Porosimetry, Permeability

25 **1 Introduction**

26 Huge amounts of construction and demolition wastes are generated and need to be treated
27 with accelerated industrialization and urbanization, especially among developing countries.
28 These regions also suffer from the depletion of natural mineral resources and the shortages of
29 waste disposal sites. Therefore, the reuse of construction waste is imperative for saving
30 natural resources, protecting the environment, and achieving sustainable development in the
31 construction industry [1]-[2].

32 In general, recycled aggregates (RA) derived from demolished concrete consist of 65–70% of
33 natural aggregates and 30–35% of old cement paste by volume [3]. **The relative residual
34 cement paste content of RA strongly depend on the porosity of the initial cement paste but it
35 is not significantly affected by the crushing process [4].** Compared to the typical natural
36 aggregates (NA) used in concrete, the adhered cement mortar on the RA has a lower density,
37 higher porosity and water absorption and lower abrasion resistance [5] [6] [7]. Besides, the
38 RA also contains more microcracks caused by the crushing process [8], and more interfacial
39 transition zones (ITZ) between old cement paste and natural aggregates [9]. The concrete
40 strength thus decreases when ~~the~~ NA are totally or partially replaced by ~~the~~ RA [8] [10].
41 Therefore, the use of recycled aggregates in the construction industry is limited [11] to road
42 pavement [12] and non-structural concrete [13].

43 To improve the properties of the RA, several techniques have been developed and can be
44 classified into two categories: (1) removing the attached mortar [14], (2) improving the
45 quality of attached paste[15]. In recent years, adopting accelerated carbonation technique to
46 improve the quality of RA has already been suggested [15],[16] [17] to densify the old cement
47 mortar attached to the RA [18] and to enhance the physical and mechanical properties of
48 recycled aggregates. The principle of this treatment is that CO₂ can react with the adhesive

49 paste on the RA, according to Equation 1 and Equation 2, to form calcium carbonate and
50 silica gel.



51 The solid volume of the adhesive paste is ~~higher~~ bigger after carbonation [1], which results in
52 a higher density and a lower absorption and porosity of RA. This increase in volume does not
53 only depends on the nature of carbonated hydrate but also on the nature of the polymorphic
54 calcium carbonate formed [19].

55 Carbonation of RA improves not only their own properties and that of RA concretes but also
56 reduces the greenhouse effect caused by the emission of carbon dioxide [8]. Using CO₂ to
57 treat recycled aggregates actually results in CO₂ storage in the adhesive paste. In practice,
58 under atmospheric conditions, concrete carbonation occurs but it could take more than 100
59 years to achieve a complete carbonation [20]. ~~It is worth noting that cement industry is one of~~
60 ~~the main sources of greenhouse gases, in particular carbon dioxide emissions [21]. Cement~~
61 ~~production generates approximately 0.8 kg of CO₂ per kg cement production, and this~~
62 ~~contributes to about 5-8 % of the global CO₂ emissions [17]. The percentage of CO₂ in~~
63 ~~cement plant fumes is approximately 15% (i.e. 370 times the percentage of CO₂ in the~~
64 ~~atmosphere).~~ It is therefore suitable to ensure accelerated carbonation of RA in an attempt to
65 rapidly improve their properties (National French Project FastCarb [21]).

66 Almost all previous studies have focused either on the physical and mechanical properties of
67 carbonated RA themselves [15] [22], or on the mechanical performance and durability of
68 concrete prepared with carbonated RA [5] [8]. ~~A significant number of studies have also~~
69 ~~focused on developing new methods to increase the efficiency of carbon dioxide~~
70 ~~sequestration: Wang et al have shown that high temperature has a significant effect on the~~

71 carbonation process [23]. Pan et al found that pretreatment with calcium hydroxide improves
 72 the efficiency of carbonation [24]. Only few studies have evaluated the impact of accelerated
 73 carbonation on the evolution of microstructure and transport properties of RA themselves.
 74 The evolution of these properties is rather complex as it results from physico-chemical and
 75 mechanical phenomena occurring at different scales, from the local environment of atoms in
 76 C-S-H to macro-cracking, the competitive effects of pores clogging which is referred to by
 77 most authors to illustrate the effect of carbonation, and those of carbonation shrinkage and the
 78 induced cracking which are poorly studied in the literature. The present study will be
 79 therefore focused on these aspects and their correlation, which constitutes the originality of
 80 this paper. Finally, it is worth specifying that due to the high variability of RA and the limited
 81 number of tests that can be performed directly on them, the experimental program will be
 82 carried out not directly at recycled concrete aggregate scale but at mortar scale representing
 83 the mortar around the natural aggregate in the recycled aggregate.

84 2 Materials and experimental program

85 2.1 Materials and samples preparation

86 Portland cement CEM I 52.5 from Villiers-au-Bouin, France was used in this study (Table 1).
 87 Its density was 3.13 g/cm³ and its specific surface area was 3,900 cm²/g.

Oxide constituents (%)									
CaO	SiO ₂	Al ₂ O ₃	MgO	Fe ₂ O ₃	SO ₃	TiO ₂	K ₂ O	Na ₂ O	P ₂ O ₃
63.70	19.60	4.50	3.90	2.30	2.60	0.20	0.70	0.13	0.20

88 **Table 1 : Chemical composition of the used cement.**

89 Natural siliceous sand (0-2 mm) with a specific gravity of 2.61 was used as aggregates. A
 90 purely siliceous sand was chosen for this study to be sure that observed calcium carbonate

91 only originates from the carbonation of the cement paste. Cement mortar was prepared with
92 mixture proportions of cement: sand: water of 1: 2.6: 0.6.

93 The water-to-cement (w/c) ratio of old concretes were relatively high before the extensive use
94 of superplasticizers, also called high-range water reducing admixtures (HRWRA). Thus a w/c
95 ratio of 0.6 was meant to be representative of old cement-based materials crushed as RA.
96 Moreover, a high w/c ratio was expected to accelerate the diffusion of carbon dioxide and
97 therefore the carbonation during the experimental study.

98 In order to explain some of the observed phenomena, a number of additional tests must be
99 carried out. These tests (indentation, XRD and TGA) should be performed on cement paste
100 due to practical limitations caused by the presence of aggregates for these experiments and
101 their analysis. As making a paste with a w/c = 0.6 causes significant segregation and bleeding,
102 a w/c ratio of 0.4 was chosen to obtain homogeneous samples.

103 Cylindrical paste samples were cast in plastic molds of \varnothing 20×50mm. Cylindrical mortar
104 samples were cast in molds with three different sizes of \varnothing 20×160mm (plastic molds), \varnothing
105 70×160mm (cardboard molds covered with plastic) and \varnothing 110×220mm (cardboard molds
106 covered with plastic). Each specimen size was used to characterize the evolution of defined
107 properties. All the samples were demolded after 24 h and then soaked in a tap water tank for
108 180 days at 23 ± 1 °C. This significant curing time was meant to reach high hydration degree,
109 so that the mortar would be more representative of old mortar attached to natural aggregates
110 in recycled concrete aggregates.

111 After the curing period, a preconditioning was carried out before carbonation tests. The
112 samples were dried at 40°C for 10 days, and then stored for another 17 days in an air-
113 conditioned room (T=20°C, relative humidity RH=55%) to homogenize the internal humidity.
114 The temperature of 40°C was chosen to dry the material without affecting the structure of

115 hydration products. The purpose of such preconditioning stage was to reach a hydric state of
116 samples close to the equilibrium with the relative humidity of the environment chosen for the
117 carbonation stage.

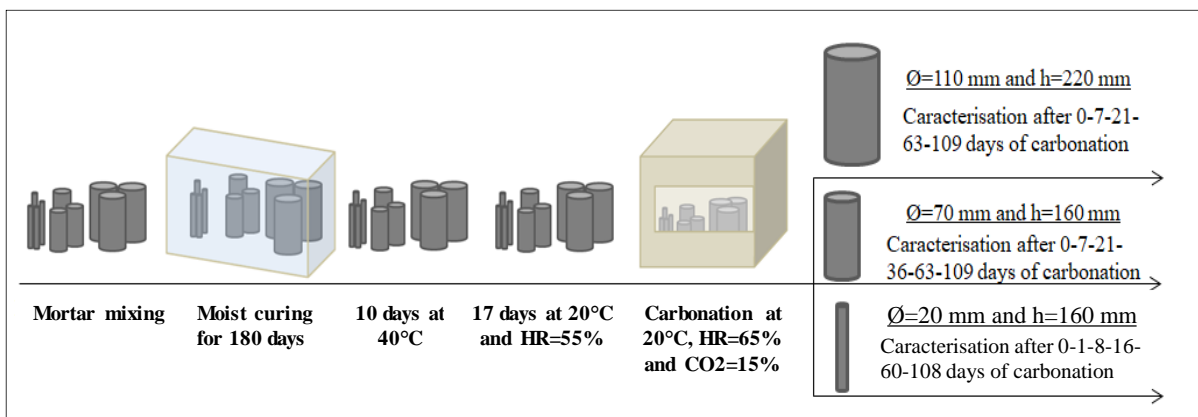
118 Some research has been done on the natural carbonation shrinkage and this has been showed
119 to cause the development of microcracks [25]. These microcracks were considered negligible
120 in the case of natural carbonation [26]. In the case of accelerated carbonation, the shrinkage is
121 faster and therefore the possibility of developing more microcracks exists. These micro cracks
122 were actually detected on samples of paste after accelerated carbonation [27] and [28]. The
123 comprehensive characterization of initially uncracked mortar samples allows highlighting the
124 specific effects of accelerated carbonation and its consequences in terms of shrinkage, tensile
125 stresses, and cracking. The mortar characterized in this study is aimed at representing the
126 mortar around NA in the RA.

127 **2.2 Accelerated carbonation procedure (treatment)**

128 Before the carbonation tests, the cylindrical-shaped mortar samples were protected
129 transversely on their bases with an adhesive tape for the medium ($\text{Ø } 70 \times 160 \text{ mm}$) and large
130 cylinders ($\text{Ø } 110 \times 220 \text{ mm}$) and a layer of resin for the small cylinders ($\text{Ø } 20 \times 160 \text{ mm}$). Then
131 they were subjected to a two-dimensional diffusion of CO_2 in a climatic chamber connected to
132 a CO_2 tank at 20°C , 65% relative humidity and 15% of CO_2 . This humidity value was chosen
133 from the literature as it would correspond to the optimum humidity for carbonation at 20°C
134 [26] [29]. The concentration of CO_2 in the chamber was controlled by an automatic CO_2
135 regulator at 15%, which is the typical CO_2 content of exhaust gases from cement
136 manufacturing process.

137 **2.3 Carbonated section proportion**

138 Each specimen size was dedicated to the characterization of specific properties. The mortar
 139 cylinders (\varnothing 20×160mm) were used to monitor the evolution of the composition through
 140 thermogravimetric analysis (TGA), the microstructure (SEM) ~~during carbonation~~ and ~~both~~
 141 ~~carbonation depth and~~ drying shrinkage ~~during carbonation~~. The mortar cylinders (\varnothing
 142 70×160mm) were dedicated to the monitoring of Young’s modulus during carbonation.
 143 Transport properties (gas permeability and porosity) during carbonation were measured on
 144 mortar cylinders (\varnothing 110×220mm). For all three sample sizes, the mass and the depth of
 145 carbonation were monitored during carbonation. The different steps through which tested
 146 specimens have gone from their mixing to carbonation test and the different characterization
 147 timelines are illustrated in Figure 1. ~~As the carbonation of small cylinders is much faster than~~
 148 ~~that of medium and large cylinders, different timelines have been set as shown in Figure 1 in~~
 149 ~~order to monitor the evolution of each size during the carbonation.~~



150

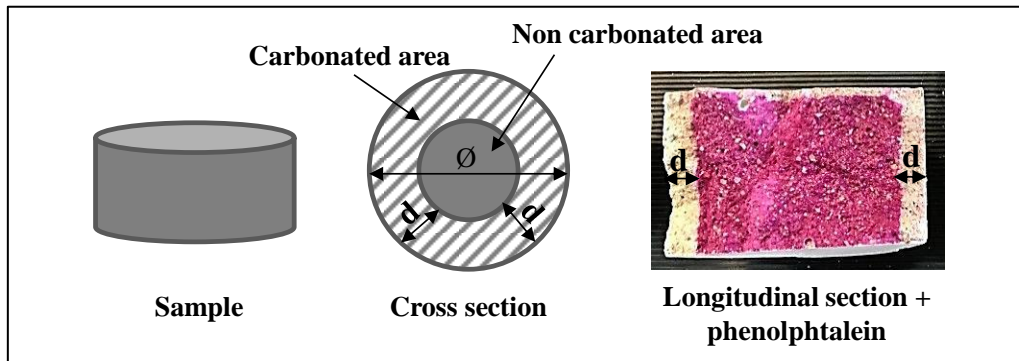
151 **Figure 1 : Schematic drawing of experiment procedure**

152 In order to correlate all the results obtained on samples of different sizes and given that
 153 carbonation is bidirectional in the present study, the parameter chosen to represent the
 154 carbonation progression was the ratio between the carbonated cross-sectional area and the

155 total cross-sectional area (Equation 3). The carbonated depth was determined using
156 phenolphthalein (Figure 2).

$$\text{Carbonated section proportion (CSP)} = \frac{\pi * (\varnothing^2 - (\varnothing - 2 * d)^2)}{\pi * \varnothing^2} * 100 \quad \text{Equation 3}$$

157 d is the carbonated depth determined using phenolphthalein test.



158

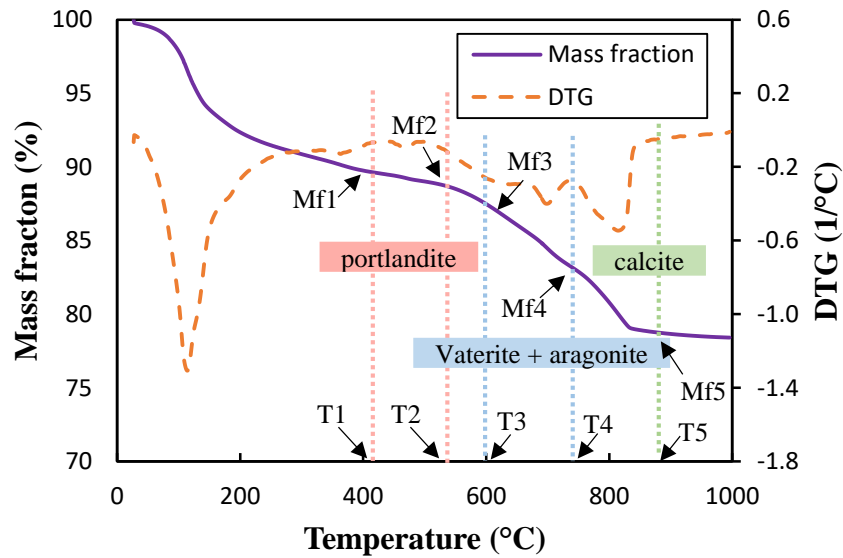
159

Figure 2 : Schematic drawing of CSP determination

160 2.4 Thermogravimetric analysis (TGA)

161 The thermal analysis was performed using a NETZSCH microbalance. A 2 cm thick sample
162 was crushed and sieved. The resulting powder sample, with a mass around 120 mg, is
163 collected in an alumina crucible and placed in the thermal balance. The tests were performed
164 under a nitrogen stream in the temperature range from 20 to 1000°C with a heating rate of
165 10°C per minute. Samples of paste and mortar were tested by TGA during their carbonation.
166 The tests performed on the paste were used to correlate the TGA results with the
167 microindentation and XRD results, while the tests performed on the mortar were used to
168 correlate the TGA results with the results of transport properties, carbonation shrinkage and
169 modulus of elasticity. Figure 3 shows an example of the TGA and derivative (DTG) curves
170 obtained.

171



172

173

Figure 3 : Treatment type model of thermogravimetric analysis curves

174

~~The graph also provides the different limit temperatures used for the identification of~~

175

~~crystallized phases. The exact boundaries temperatures were determined using the derivative~~

176

~~curves, basing on several guidelines [29]–[30]. Many authors have identified the~~

177

decomposition temperature ranges of the phases of cement-based materials [29] [30]. These

178

temperatures are likely to vary as a function of measurement parameters (heating rate, number

179

of measuring heads, type of sample holder) or the sample.(compactness, mass, **carbonation**

180

rate) [31] [32] [33]. Therefore, in this study, the limit temperatures T_i are clearly defined by

181

the edges of the characteristic peaks of the DTG curve [26] [33] [34] (Figure 3).

182

The contents of portlandite CH, vaterite + aragonite, and calcite (percentage by mass in the

183

sieved mortar) are calculated on the basis of Equation 4, Equation 5 and Equation 6

184

respectively.

$$CH = (M_{CH}/M_{H_2O}) \cdot (M_{f1} - M_{f2}) \quad \text{Equation 4}$$

$$\text{Vaterite+aragonite} = (M_{CaCO_3}/M_{CO_2}) \cdot (M_{f3} - M_{f4}) \quad \text{Equation 5}$$

$$\text{Calcite} = (M_{CaCO_3}/M_{CO_2}) \cdot (M_{f4} - M_{f5}) \quad \text{Equation 6}$$

185 Where M_{fi} is the mass fraction corresponding to the limit temperatures T_i determined using
186 the DTG curve as mentined above (Figure 3). M_{CH} , M_{H_2O} , M_{CO_2} and M_{CaCO_3} are respectively
187 the molar mass of $Ca(OH)_2$, H_2O , CO_2 , and $CaCO_3$ ($M_{CH}=73\text{g/mol}$; $M_{H_2O}=18\text{g/mol}$;
188 $M_{CO_2}=44\text{g/mol}$; $M_{CaCO_3}=100\text{g/mol}$).

189 2.5 Measurement of shrinkage

190 2.5.1 Drying and carbonation shrinkage:

191 The shrinkage of the mortar was measured on cylindrical samples with a diameter of 20 mm
192 and a height of 160 mm. The samples were equipped with metal studs placed in the mold at
193 each end before casting. These studs made it possible to place the cylinder in a vertical sensor
194 to measure the longitudinal deformation with a precision of 0.02 mm. ~~which allowed the~~
195 ~~cylinders to be placed in the vertical sensor with a precision of 0.02mm.~~ The measurements
196 ~~longitudinal deformation~~ were automatically ~~measured~~ recorded using the USB-ITPACK
197 software.

198 After the 180-day curing, the shrinkage was measured during preconditioning step (10 days at
199 40°C and 17 days at 20°C , see section 2.1). Then shrinkage was measured during the
200 carbonation stage in the carbonation chamber ($T = 20^\circ\text{C}$, % $CO_2 = 15\%$ and $RH = 65\%$) and
201 the air-conditioned room ($T = 20^\circ\text{C}$, % $CO_2 = 0.04\%$ and $RH = 55\%$). Shrinkage
202 measurements were recorded continuously for 3 months of carbonation.

203 **2.6 Transport properties measurements**

204 **2.6.1 Porosity accessible to water**

205 Total porosity (i.e. the volumetric proportion of voids) was determined under vacuum
206 according to the French standard NF P18-459. The slices were placed in a desiccator under
207 vacuum for 4 hours (± 30 min), then the desiccator was filled with water for 44 hours (± 30
208 min). The slices were then dried at 105°C to constant weight. The following weights were
209 recorded:

210 • W_{dry} : dry weight of the sample, after oven-drying at 105°C .

211 • W_{sat} : weight in air of saturated-dry surface sample.

212 • W_{hydro} : hydrostatic weight, weight in water of saturated sample.

213 The total porosity is then obtained from the following Equation 7:

$$\text{Porosity (\%)} = \frac{W_{sat} - W_{dry}}{W_{sat} - W_{hydro}} * 100 \quad \text{Equation 7}$$

214 The test was carried out at each characterization time on two samples ($\emptyset=110\text{mm}$; $h = 3\text{cm}$).

215 The samples were sawn from two different cylinders.

216 **2.6.2 Mercury intrusion porosimetry**

217 Carbonation modifies the total porosity and the pore size distribution of cement-based
218 materials. Pore sizes have a direct influence on transport properties such as permeability [35].

219 For that purpose, a standard porosimeter which allows the application of pressures up to 400
220 MPa has been used. This corresponds to a minimum pore radius of 1.5nm. Assuming that
221 pores are cylindrical, the radius r , penetrated by mercury at pressure P , can be calculated by
222 the Washburn Equation 8:

$$r = \frac{2 \cdot \sigma \cdot \cos(\theta)}{P}$$

Equation 8

223 with σ the surface tension of the mercury ($\sigma = 0.475 \text{ N / m}$) and θ the contact angle between
 224 the solid surface and the mercury ($\theta = 141^\circ$).

225 Mercury intrusion porosimetry was performed on small pieces of mortar (3 to 5 mm) dried in
 226 an air-conditioned room at 20°C and 50% RH for 24 hours before the test. Those latter were
 227 taken from the carbonated and non-carbonated zone for two different **carbonated section**
 228 **proportion** (CSP=15% and CSP= 55%).

229 **2.6.3 Gas permeability**

230 The test consists in applying a constant pressure gradient to a sample ($\varnothing=110 \text{ mm}$; $h=50 \text{ mm}$)
 231 and measuring the gas flow through the sample at equilibrium. 2 samples were tested at each
 232 stage. It is then possible to calculate the apparent permeability which depends on the applied
 233 overpressure. The test was carried out at overpressures of 1bar, 1.6 bar, 2 bar and 2.4 bar.

234 The apparent and intrinsic permeabilities were measured after 7 days (K7) and 28 days (K28)
 235 of drying at 80°C and after a total drying at 105°C (Kdry). At each characterization time, 2
 236 samples were tested. Samples were sawn from two different cylinders of the same size. For
 237 each sample and each pressure the apparent permeability was calculated from Equation 9.

$$K_a = \frac{Q_1 \cdot 2 \cdot \mu \cdot L \cdot P_{atm}}{S(P_1^2 - P_{atm}^2)}$$

Equation 9

238 Q_1 : volume flow at the inlet (m^3/s)

239 μ : dynamic viscosity of nitrogen (Pa.s)

240 P_1 : injection pressure (Pa)

241 P_{atm} : atmospheric pressure (Pa)

242 L : thickness of the sample (m)

243 S: section of the sample (m²).

244 From the apparent permeability measurements the intrinsic K_v permeability can be deduced

245 according to Klinkenberg's approach (1941) (Equation 10).

$$K_a = K_v \left(1 + \frac{\beta}{P_m} \right) \quad \text{Equation 10}$$

246 P_m: Mean pressure, equal to (P₁ + P_{atm}) / 2

247 β: Klinkenberg's coefficient.

248 **2.7 Mechanical properties**

249 **2.7.1 Elastic modulus**

250 The static modulus of elasticity (E) of mortar was assessed on the cylindrical specimens

251 (Ø=70 ×140mm) in accordance with the ASTM C 469-65 at different carbonation rates. The

252 average of 3 values was considered at each characterization time.

253 **2.7.2 Microhardness**

254 In a microindentation test, a diamond indenter of specific geometry is impressed into the

255 surface of the samples using a known applied load. The microindenter monitors and records

256 the load and the displacement of the indenter and provides an indentation load–depth curve.

257 The indentation load at the peak indentation depth can be used as a manifestation of the

258 surface hardening of the samples.

259 In this study, a Fischer digital microhardness tester (FISCHERSCOPE HM2000) was used to

260 measure the microhardness at the surface of the **paste** sample at each characterization. The

261 microindentation test was carried out on paste instead of mortar to avoid the effect of sand

262 particles. The 20mm thick paste sample was first finely polished to meet the experimental

263 requirements of the digital microhardness tester.

264 The indenter was initially at the center of the cylindrical sample (abscissa $X=0\text{mm}$) and then
265 moved towards the edge of the sample (abscissa $X=10\text{mm}$). On this 10mm linear path, 102
266 indentations were performed. At each indentation a force of 300 N was imposed for 10s and
267 the value of the depth reached by the indenter was used to characterize the hardness of the
268 sample at this point.

269 **2.8 X-Ray diffraction**

270 XRD analyses were carried out on a Malvern Panalytical Aeris instrument. It combines two
271 technologies from Aeris and Zetium and provides full material characterization by adding
272 information about elemental composition determined by Zetium to the phase identification
273 from Aeris.

274 Scanning program consisted in rotating between 7 and $70^\circ 2\theta$ with a step size of $0.01^\circ 2\theta$ and
275 a time per step of 480.165 ms.

276 XRD analysis was performed on paste instead of mortar to avoid the effect of sand particles,
277 **as many peaks associated to quartz sand would have appeared in results.** The measurements
278 were carried out on three samples at different stages of carbonation: before carbonation, after
279 3 days of carbonation and after 6 days of carbonation.

280 **2.9 Microstructural observation**

281 The morphologies of the representative mortar before and during accelerated carbonation
282 were observed via a scanning electron microscopy with energy dispersive X-ray spectroscopy
283 (SEM-EDX).

284 For each observation, a 2cm thick sample was put in the resin for 48 hours. Then the surface
285 of the sample was polished and covered with a gold layer before SEM observations in order to

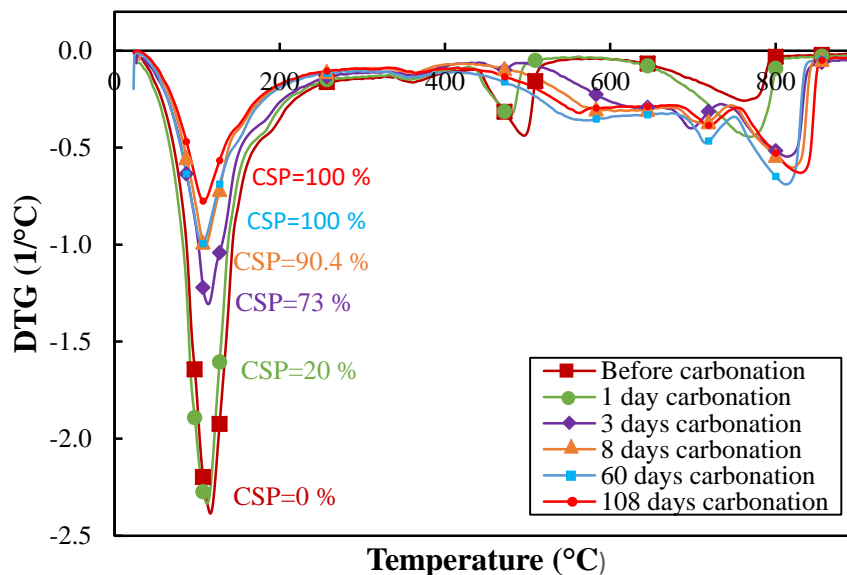
286 obtain clear images and to facilitate the identification of the different components present and
287 formed during carbonation.

288 3 Results and discussion

289 3.1 Microstructure and properties of formed phases

290 3.1.1 Thermogravimetric analysis

291 Figure 4 shows the results of analyses performed on samples of mortar at different
292 carbonation times in terms of carbonated section proportion (CSP). For uncarbonated samples
293 (CSP=0%), two negative peaks can be distinguished after 200°C. These are related to the
294 decomposition of portlandite CH (around 450-550°C [36]) and calcium carbonate (around
295 550-950°C [37]). CaCO_3 Calcite was present, in a small amount, in raw samples, because of
296 the usual reaction of cement pastes with atmospheric CO_2 prior to the carbonation treatment.

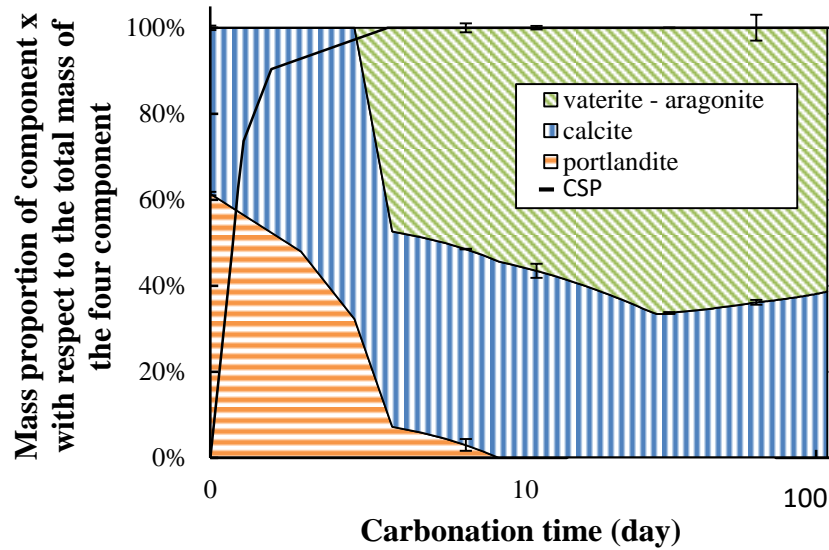


297

298 **Figure 4 : Thermogravimetric analysis curves (DTG) of carbonated mortar at different**

299

carbonation ages.



300

301 **Figure 5 : Carbonation of mortar:** Evolution of the mass distribution of the four components (calcite,
 302 portlandite, vaterite, and aragonite) with respect to the total mass = mass of calcite + mass of portlandite + mass of
 303 aragonite + mass of vaterite

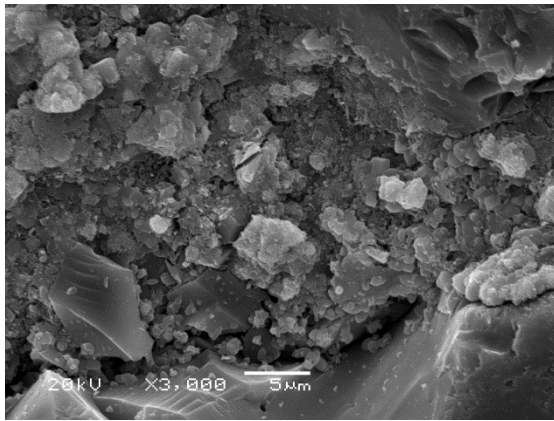
304 As the carbonation progressed (CSP increase), it is noteworthy that the portlandite peak
 305 rapidly decreased ~~so that it completely and completely~~ disappeared after 8 days of carbonation
 306 (CSP=90.4%) while the peak of ~~calcium carbonate~~ calcite significantly increased at the same
 307 time. ~~Precipitated calcite particles can be detected by SEM after 1 day of carbonation~~ (Figure
 308 6-b). After the first 8 days the amount of calcite (Figure 5) remained almost constant as the
 309 carbonation progressed while two new peaks corresponding to the other two polymorphs of
 310 calcium carbonate: vaterite and aragonite developed (Figure 4) [29].[34] The more the
 311 carbonation advanced, the larger these peaks and the wider the mass loss temperature range
 312 became.

313 The type of calcium carbonate polymorph formed depends on the type of hydrates affected by
 314 carbonation and consequently on the pH of the pore solution. The carbonation of portlandite
 315 initially dominates. As long as Portlandite ~~has is~~ not ~~fully completely~~ dissolved, it maintains a
 316 basic pH of the interstitial solution around 12.5 due to its important buffering effect [26]. At

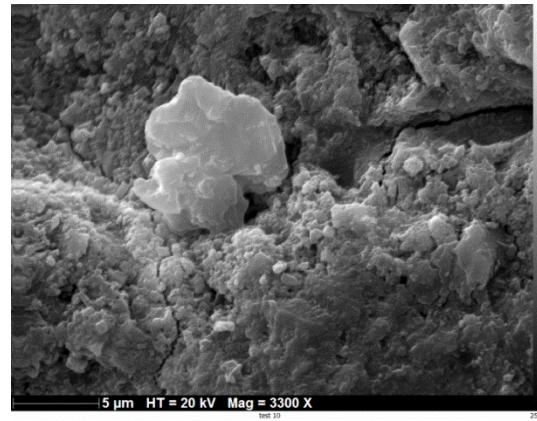
317 this stage of carbonation, calcite – the stable polymorph of calcium carbonate – is the
318 dominant polymorph formed during carbonation [38] [39] as seen in Figure 4 and Figure 5. Its
319 decarbonation took place between 720 and 960°C [36]. As carbonation progresses, portlandite
320 is depleted and the remaining particles are covered by calcite crystals. As a result, its
321 carbonation becomes very slow compared to other hydrates, especially C-S-H [23]. However,
322 since C-S-H have no buffering effect, their carbonation induces a decrease in the pH of pore
323 solution to lower than 9 [40]. The formation of other polymorphs (vaterite, aragonite)
324 becomes therefore predominant [41] as seen in Figure 5 after almost 8 days of carbonation.
325 These two polymorphs decompose between 550 and 720°C (Figure 4) which suggests a
326 poorly-crystalline [36] and less stable [42] phase.

327 The formation of vaterite is more pronounced than aragonite during the carbonation of CSH
328 [38]. This is confirmed by TGA results and SEM observations. Figure 6 after 16 and 60 days
329 of carbonation shows the significant precipitation of vaterite. In fact, vaterite has no distinct
330 morphology, in agreement with the literature data [43] [44]; its formation occurs as sub- μm -
331 sized spherical particles as seen in Figure 6-c. The detection of aragonite which have needle-
332 shaped crystal morphology [43] [44] was difficult on all the images obtained. Concerning
333 ~~TGA results the aragonite peak was observed after 109 days of carbonation (figure 4)~~
334 ~~(between 500 and 600°C).~~

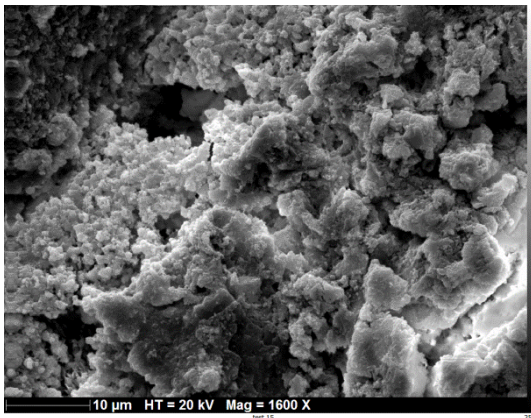
335



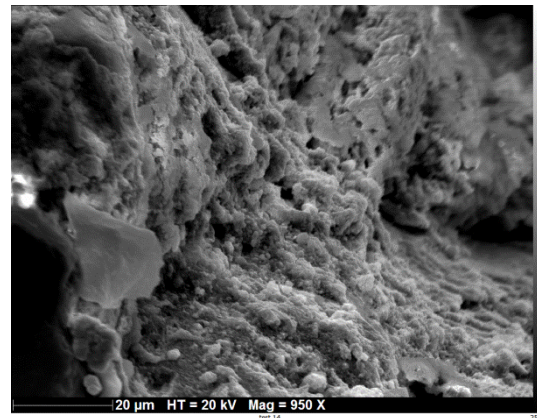
a) Before carbonation (CSP=0%)



b) 1 day carbonation (CSP=20%)



c) 16 days carbonation (CSP=100%)



d) 60 days carbonation (CSP=100%)

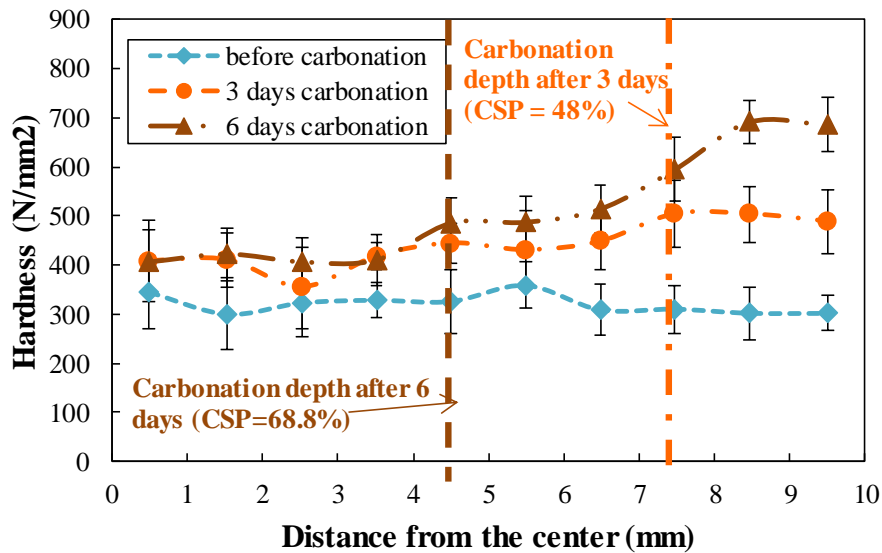
336

Figure 6 : SEM images after different carbonation ages.

337 The last observation concerns the temperature limits. It was not possible to establish a precise
 338 temperature, which limits the temperature range of the portlandite decomposition and calcium
 339 carbonate precipitation [33]. It is noteworthy to mention that these temperatures are not fixed
 340 for each component, especially for calcium carbonate and, moreover, the corresponding peak
 341 is shifted as the carbonation proceeds. This aspect, illustrated in Figure 4 ~~for calcite, aragonite~~
 342 ~~and vaterite peaks~~, can be explained by the particle size of the calcium carbonate ~~that is~~
 343 ~~influenced by the thermal dissociation of calcium carbonate~~ [33]. As carbonation advances,
 344 the particles of calcium carbonate become denser and therefore their dissociation temperature
 345 increases [33].

346 **3.1.2 Microhardness**

347 The micro indentation test was carried out on paste as already indicated to avoid the effect of
348 sand particles. Figure 7 shows the change in hardness as a function of the distance from the
349 center of the polished cylinder after three carbonation times: before carbonation, after 3 days
350 and 6 days of accelerated carbonation. In order to understand its evolution, DRX (Figure 8)
351 and TGA (Figure 9) tests were carried out on paste at the same time of carbonation as of
352 microindentation. The dotted lines on the curves represent the boundary between the
353 carbonated area and the non-carbonated area detected by the phenolphthalein indicator on
354 paste specimens.



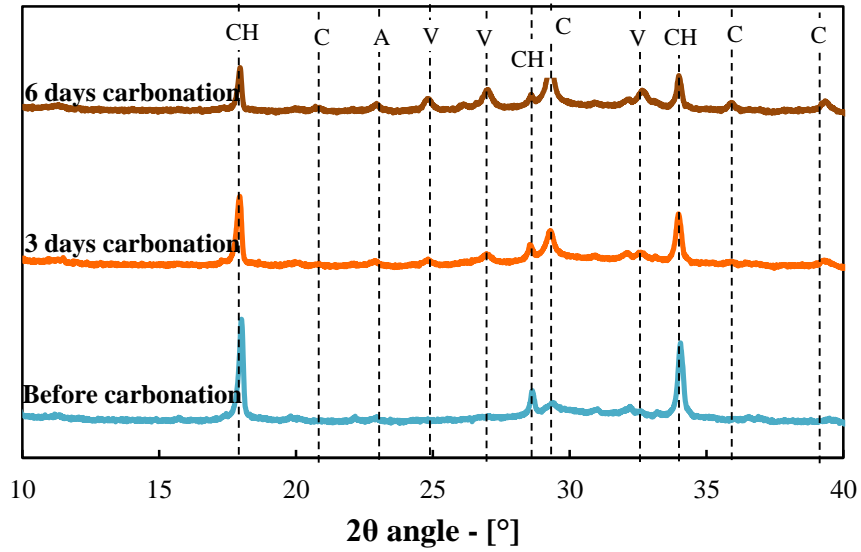
355

356 **Figure 7 : Evolution of the microhardness of the cement paste during carbonation**

357 The first curve corresponds to the hardness before carbonation of a sample along the radius
358 (from center: X = 0 mm to edge: X = 10 mm). The value of hardness is constant with a very
359 small reduction at the edge due to an edge effect. The second curve obtained after 3 days of
360 carbonation shows a gradual increase from the center to the edge. The hardness of the
361 carbonated zone detected by phenolphthalein (dotted line on the graph X = 7.4mm) has
362 undergone the greatest increase. It is noteworthy that the zone where hardness significantly

363 increased was larger than the zone with low pH ~~as indicated~~ detected by phenolphthalein. The
364 third curve obtained after 6 days of carbonation reveals a strong increase in the hardness at the
365 edge. At the center, hardness did not significantly increase from 3 days to 6 days. The fact
366 that the carbonated zone detected by phenolphthalein (dotted line on the graph $X = 4.7\text{mm}$)
367 undergoes the greatest increase is in agreement with the curve obtained after 3 days of
368 carbonation. It has been observed that the measured microhardness of the cement pastes in the
369 carbonated zone, was higher than that of the non-carbonated [45]. ~~As the carbonation~~
370 ~~progresses, the evolution of the composition of the paste (Figure 8 and Figure 9) and~~
371 ~~consequently the physicochemical properties of the cementitious material causes a~~
372 ~~modification at the level of the microstructure of cement paste [46] [47] [48] [49]. These~~
373 ~~microstructural changes help to discuss the evolutions of mortar properties that were~~
374 ~~monitored in this study such as the transport properties [46] [47] and mechanical properties~~
375 ~~[46]. The improvement of mechanical properties in carbonated area could be expected [46]~~
376 and this is consistent with the significant calcium carbonate formation after 3 and 6 days of
377 carbonation shown in Figure 9. Such precipitation, concentrated at the edge of the ~~paste~~
378 sample [26] [29], is responsible for the clogging of the pores and the healing of the cracks that
379 increase the hardness of the concerned area.

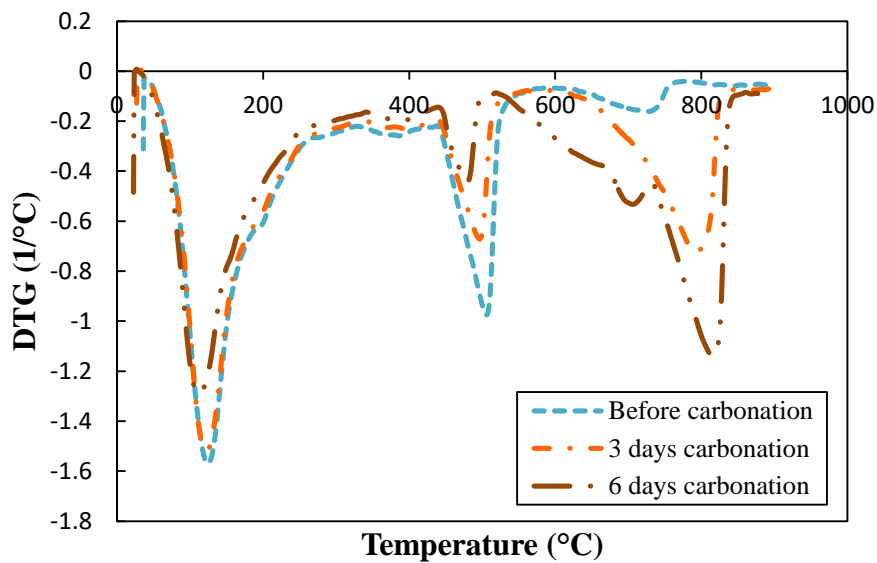
380 Figure 8 also shows that calcium carbonate precipitates into different polymorphs. However,
381 the precipitation of these polymorphs is not simultaneous. After 3 days, calcium carbonate is
382 mainly formed as calcite ($2\theta = 29.4$ and 39.4 [37]) whereas after 6 days vaterite and aragonite
383 are also present. These results are in consistent with the results of DTG analysis in Figure 9,
384 the two peaks ~~which appear after 6 days of carbonation~~ between 550°C and 720°C correspond
385 to the precipitation of the poorly crystallized CaCO_3 as vaterite and aragonite ~~from the~~
386 ~~carbonation of C-S-H~~ [37].



387

388

Figure 8 : XRD of paste during carbonation



389

390

Figure 9 : DTG of paste during carbonation

391 It is worth noting that polymorphs of calcium carbonate have different hardness and elastic
 392 modulus [43]. Vaterite has the highest hardness and elastic modulus (elastic modulus E found
 393 to be in the ranges of 16 to 61 GPa), then calcite (E found to be in the ranges of 6 to 41GPa)
 394 and finally aragonite (E found to be in the ranges of 2 to 34 GPa) [43]. The effect of this
 395 difference in hardness and elastic modulus between the polymorphs appears on the curve

396 obtained after 6 days of carbonation in Figure 7. The significant increase in the hardness of
397 the carbonated zone after 6 days of carbonation can be explained by the formation of vaterite
398 detected by TGA, which exhibits higher value of hardness compared to the calcite formed
399 after 3 days of carbonation.

400 Negative effects of the increase in hardness can also be pointed out. The carbonated zone
401 actually becomes more vulnerable to stress-inducing phenomena such as drying and more
402 brittle and thus more sensitive to the propagation of cracks [28] [50]. On the other hand, the
403 existence of two separated zones having different elastic modulus in a not fully carbonated
404 surface, can also induce the development of tensile stresses between the surface and the core
405 of the sample. Consequently, cracks or microcracks may be generated. The development of
406 tensile stresses is not constant during the carbonation. Due to structural effect, it initially has
407 low values before increasing until reaching a peak and decreasing after stress relaxation due
408 to cracking and ~~finally due to a~~ complete carbonation of the specimen.

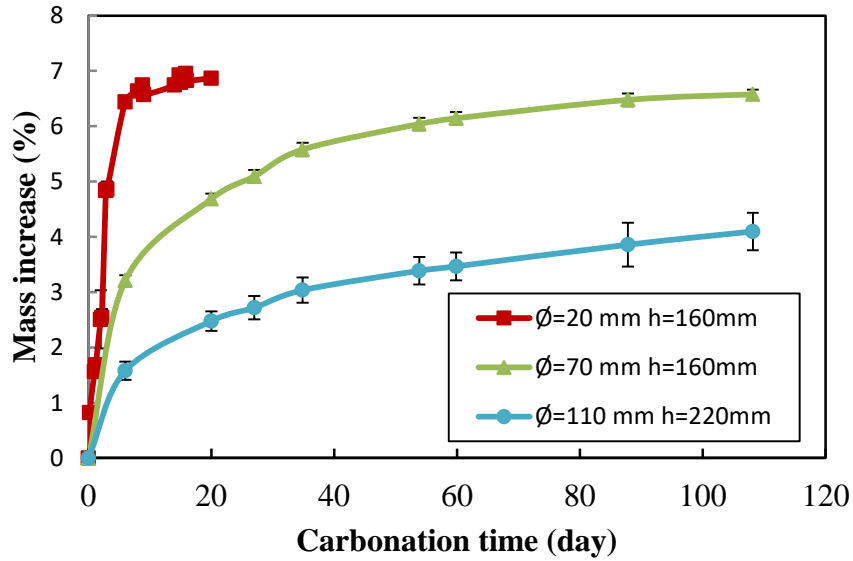
409 **3.2 Macroscopic properties and time-dependent behaviour**

410 **3.2.1 Mass gain and carbonation rate**

411 Figure 10 shows the evolution of the mass of the three sample sizes during carbonation. The
412 mass increase is calculated from Equation 11.

$$\text{Mass increase (t)} = \frac{\text{mass after carbonation of time } t - \text{mass before carbonation}}{\text{mass before carbonation}} \quad \text{Equation 11}$$

413 The increase in mass observed was very pronounced at the initial stage of carbonation than it
414 became slower. The stabilization period depends on the size of the samples. This stabilization
415 was faster when the sample size was smaller. It began after 8 days for small cylinders
416 ($\text{Ø}=20\text{mm}$; $h=160\text{mm}$), 60 days for medium-sized cylinders ($\text{Ø}=70\text{mm}$; $h=160\text{mm}$), while for
417 large cylinders ($\text{Ø}=110\text{mm}$ $h=220\text{mm}$) the mass was still increasing after 110 days.



418

419

Figure 10 : Mass gain during carbonation as a function of carbonation time

420

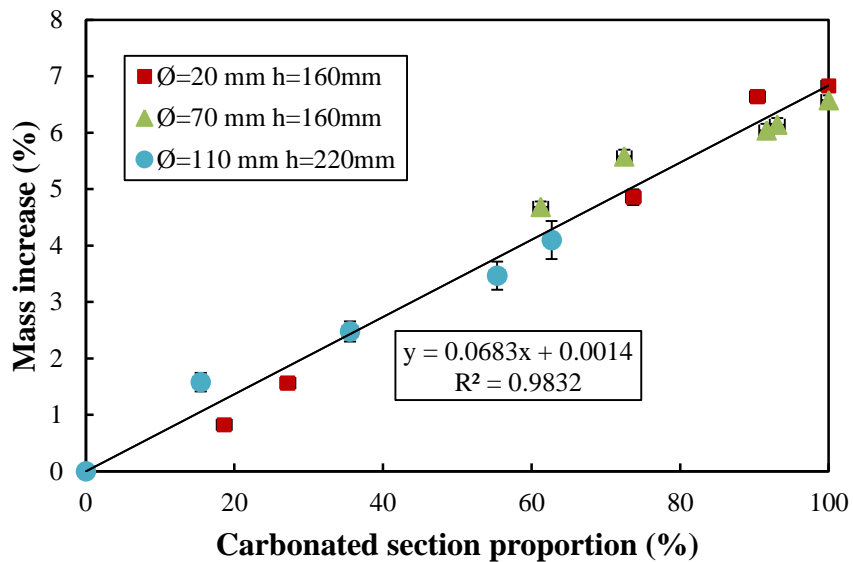
To relate the results of tests carried out on samples of different sizes, the **carbonated section**

421

proportion was defined (see section 2.3). Figure 11 shows the evolution of the mass of

422

samples of different sizes as a function of the **carbonated section proportion**.



423

424

Figure 11 : Mass gain as a function of the carbonated section proportion

425

With respect to this parameter, the mass increase curves of the samples of different sizes **are**

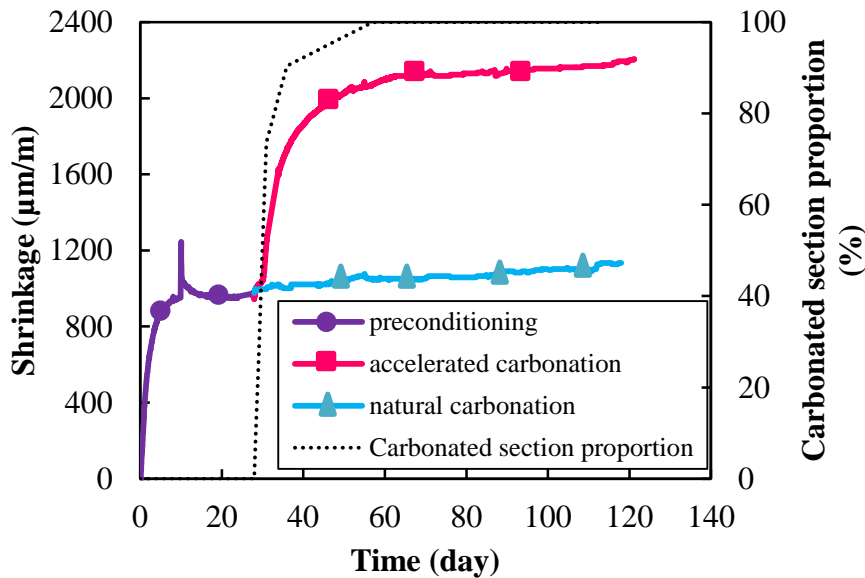
426

very close and follow the same linear increase (Figure 11). This validates the possibility of

427 using the **carbonated section proportion** defined in previous section as an indicator of the
428 progress of physico-chemical transformation to be correlated to the evolution of other
429 properties regardless of the size of the sample.

430 3.2.2 Shrinkage of mortar during carbonation

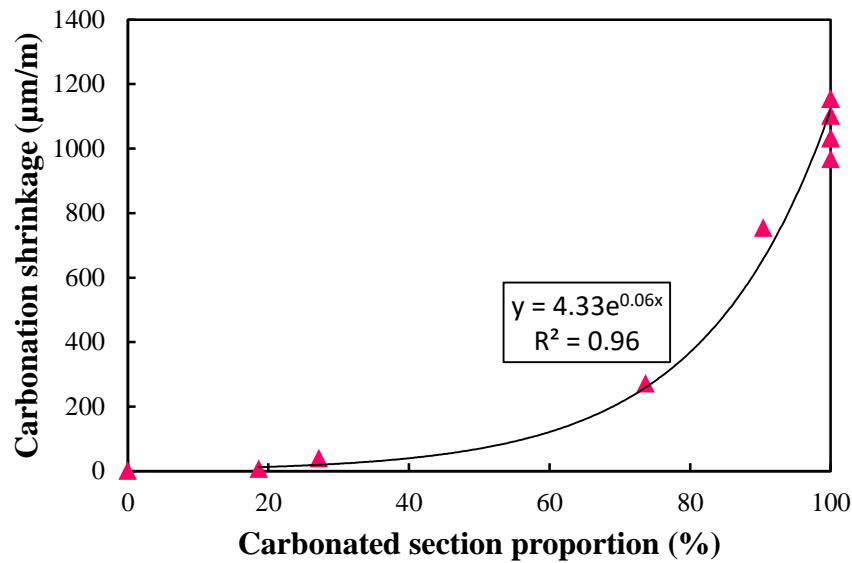
431 Figure 12 displays both drying and carbonation shrinkage that occur during the
432 preconditioning step and carbonation tests respectively.



433

434 **Figure 12 : Shrinkage of mortar during preconditioning and carbonation**

435 The shrinkage during the first 27 days corresponds to the drying shrinkage associated to the
436 preconditioning. After preconditioning, the bottom curve corresponds to the shrinkage of the
437 sample placed in the air-conditioned room and undergoing natural carbonation while the top
438 curve corresponds to the shrinkage of a sample undergoing accelerated carbonation in the
439 carbonation chamber. In the air-conditioned room, a stabilization of shrinkage was observed
440 at this time scale while it significantly increased in the carbonation chamber. The difference
441 between the shrinkage curves after 27 days can thus be attributed to the accelerated
442 carbonation shrinkage.



443

444

Figure 13 : Carbonation shrinkage vs carbonated section proportion

445 The shrinkage curve showed the same evolution as the **carbonated section proportion** curve

446 (dotted curve Figure 12). Figure 13 shows the evolution of the carbonation shrinkage as a

447 function of **carbonated section proportion**. Shrinkage slightly increased at the first day of

448 carbonation when CSP increased from 0 to 20%; a more significant increase of shrinkage was

449 observed for the next few days when CSP increased from 20 to 90%. Then the shrinkage

450 begins to stabilize. As reported in the literature, carbonation shrinkage results from the

451 decalcification and polymerization of C-S-H followed by the formation of amorphous silica

452 gel [26] [29] [51]. **The decalcification** and polymerization of CSH cause a tension in the

453 carbonated zone. This leads to a differential shrinkage between the surface and the core of the

454 concrete (carbonation shrinkage). These results were recently confirmed in the work of

455 Kangni-Foli [52], that showed on model paste using NMR results, TGA results and

456 carbonation shrinkage measurements that shrinkage increases with the decalcification level of

457 C-S-H. This unambiguously confirms that the shrinkage generated by carbonation is due to

458 decalcification of C-S-H and polymerization of silica chains [52]. Such mechanisms may

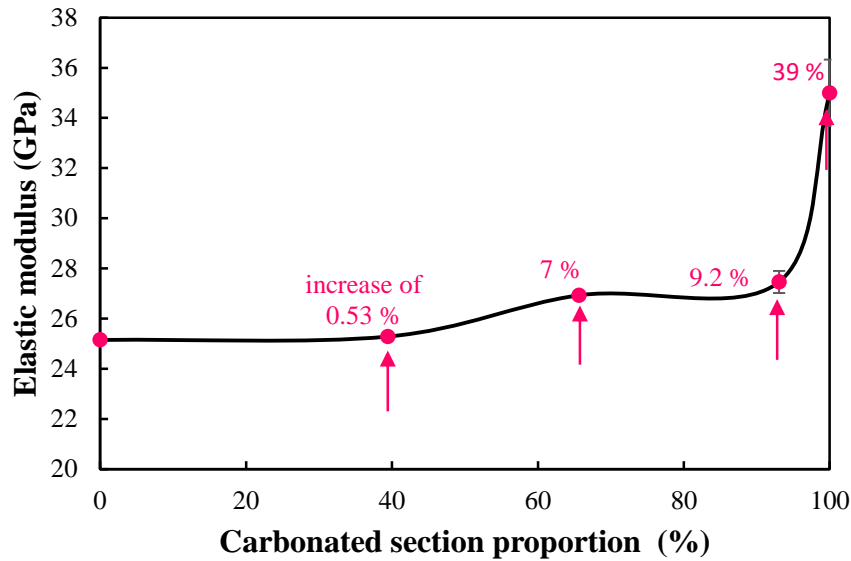
459 explain the slight increase in shrinkage at the first day of carbonation given that portlandite

460 carbonation is dominant compared to that of C-S-H [51]. This large amount of portlandite
461 present at the start of carbonation plays a protective role, it protects C-S-H from carbonation
462 and therefore provides some kind of mechanical protection (decreases carbonation shrinkage)
463 [38]. While the amount of portlandite sharply decreases (Figure 4 and Figure 5) after the first
464 day of carbonation, the carbonation of CSH becomes predominant and results in a significant
465 carbonation shrinkage. After 8 days of carbonation (CR = 90.4%), most of hydration products
466 (especially portlandite and C-S-H) have been carbonated so that the shrinkage begins to
467 stabilize.

468 It is worth specifying that the shrinkage caused by carbonation (approximately 1000 $\mu\text{m}/\text{m}$)
469 was significant and reached a value almost equal to drying shrinkage. Such differential
470 shrinkage can cause the development of micro cracks in the carbonated zone as seen in Figure
471 6-b [26] [28] [53].

472 **3.2.3 Elastic Modulus**

473 The effects of carbonation on the elastic modulus of mortar are shown in Figure 14. The
474 enhancement in elastic modulus with the increase in CSP as observed in Figure 14 [19] [46]
475 [54] leads to a stiffer cement mortar [46]. During accelerated carbonation tests, the hydrated
476 cement matrix is densified and the pore structure is refined due to the precipitation of the
477 formed calcium carbonates [18] [55]. It is also well known that calcium carbonate is an
478 excellent binder [56] providing most of the mechanical resistance of lime mortars [19].



479

480

Figure 14 : Elastic modulus of mortar during carbonation

481 The increase in elastic modulus was not proportional to the carbonation rates [46]. For CSP
 482 varying from 0 to 40%, a slight increase of 0.53% was observed. The precipitation of calcium
 483 carbonate results in an increase in the volume of the solid phase. At this stage, two zones of
 484 different elastic modulus can be present in addition to the transition zone between them. This
 485 profile of elastic modulus associated to stresses due to carbonation shrinkage was likely to
 486 cause the development of tensile stresses in the external part of the sample. The carbonation
 487 actually makes the carbonated zone more prone to cracking [28] [53]. During this first step of
 488 carbonation contradictory mechanisms can develop in the cement paste: clogging of the pores
 489 and cracking. The tests results suggest that the effects of both mechanisms nearly
 490 compensated during this stage: positive effect of calcium carbonate formation ~~as observed in~~
 491 ~~Figure-7~~, and the negative effect of the microcracks, which could explain the limited increase
 492 in the modulus of elasticity during the first part of carbonation.

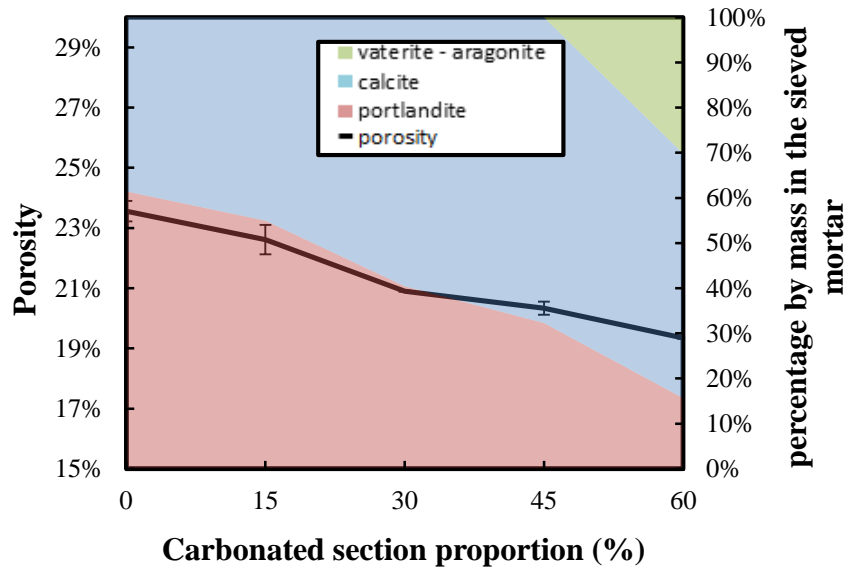
493 For CSP varying from 40% to 93%, the increase became higher and the elastic modulus
 494 reached a value of 27.5 GPa. During the last stage of carbonation in terms of CSP (from 93 to
 495 100%), the elastic modulus reached a value of 35.8 GPa. At this stage the possible cracks

496 have already developed. At the same time the clogging effect continues, but its rate can be
497 lower for several reasons: the drop in the amounts of carbonatable hydrates, the formation of
498 calcite crystals around the portlandite particles making it difficult to reach it [29] and the
499 decrease in the CO₂ diffusion coefficient after clogging of pores [26]. In this case the clogging
500 not only reduces the volume of the pores but at the same time ensures the healing of
501 microcracks already present or developed during carbonation [57] [58]. In addition,
502 carbonation shrinkage of the inner part of specimens can cause the closure of cracks
503 developed in the outer area. Thus, at this stage, the clogging dominate the cracking effect,
504 moreover the vaterite formed from C-S-H has higher modulus than calcite, which **could also**
505 explain the significant increase in the elastic modulus of the material **at this stage**.

506 **3.3 Transport properties**

507 **3.3.1 Porosity and pore sizes**

508 Figure 15 shows a decrease in connected open porosity as carbonation progresses. It goes
509 from 23.6% to 19.3% when the CSP increases from 0 to 60%. Such results are expected and
510 they are in agreement with those reported in literature [26] [46] [56] [59] [46]. During
511 carbonation the formation of calcium carbonate causes the clogging of pores and the reduction
512 in total porosity [19] [26] [46]. [25] [60]. This increase in volume depends on the nature of the
513 polymorphic calcium carbonate formed. Houst [19] mentioned that during the carbonation of
514 portlandite if the calcium carbonate precipitates in the form of calcite, an increase of 12% in
515 volume is expected while it is around 19% in the case of formation of vaterite and around 3%
516 in the case of formation of aragonite.



517

518

Figure 15 : Evolution of the porosity of the mortar during carbonation

519 More than simply reducing the total porosity, carbonation modifies the pore size distribution.

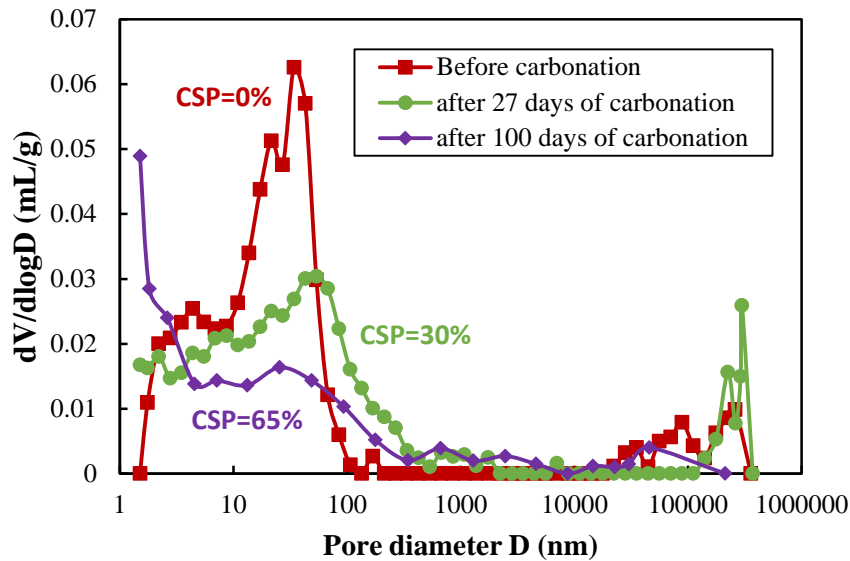
520 Figure 16 shows the evolution of the pore distribution during carbonation. Three carbonation

521 times were chosen to be characterized: the distribution of pores before carbonation (CSP =

522 0%), after 27 days of carbonation (CSP = 30%) and after 100 days of carbonation (CSP =

523 67%). In these last two cases (CSP = 30% and CSP = 67%) the sample was taken from the

524 carbonated zone.



525

526

Figure 16 : Impact of carbonation on the pore size distribution

527 The results obtained by mercury porosimetry reveal a decrease in the volume of the
 528 mesopores with an access diameter $D < 50$ nm. This decrease can be attributed to the
 529 formation of calcium carbonate in the pores during carbonation. The formation of a
 530 macroporosity ($50 \text{ nm} < D < 550 \text{ nm}$ and $D > 22000 \text{ nm}$) can be also distinguished. This
 531 increase in the macroporosity could be explained by two phenomena:

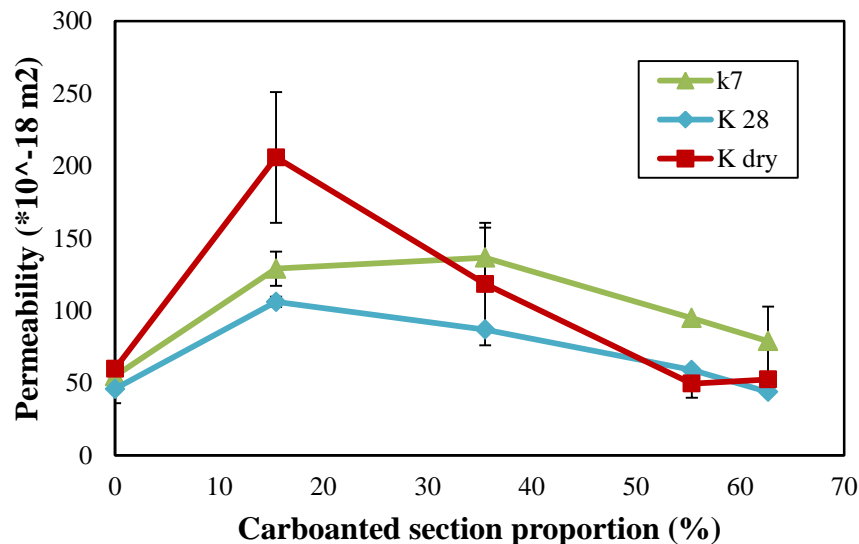
- 532 - The formation of microcracks in the carbonated zone which becomes more brittle and
 533 subjected to stress development during carbonation (section 3.1.2). These microcracks
 534 result from the carbonation shrinkage and the tensile stresses developed between the
 535 carbonated and non-carbonated zone [19] [29].
- 536 - The structure of the silica gel resulting from the carbonation of the C-S-H. The
 537 porosity of silica gel being around 100 nm could therefore be at the origin of
 538 macroporosity formation identified [29] [61].

539 This macroporosity was higher in the sample carbonated for 27 days (CSP = 30%) than in the
 540 sample carbonated for 100 days. During the first stages of carbonation, several phenomena
 541 contribute to the significant formation of macropores. Then, after the progress of carbonation,

542 the precipitation of calcium carbonate begins to dominate and leads to the healing of cracks.
543 In addition, carbonation shrinkage of the inner area of the cross section can cause the closure
544 of cracks developed in the exterior area and hence the closing of the macropores.

545 3.3.2 Gas permeability

546 Figure 17 presents the evolution of the gas permeability during carbonation. Three values of
547 intrinsic permeability were determined for each CSP considered: permeability after 7 days of
548 drying at 80°C (K7), permeability after 28 days of drying at 80°C (K28) and permeability
549 after a total drying at 105°C (Kdry).



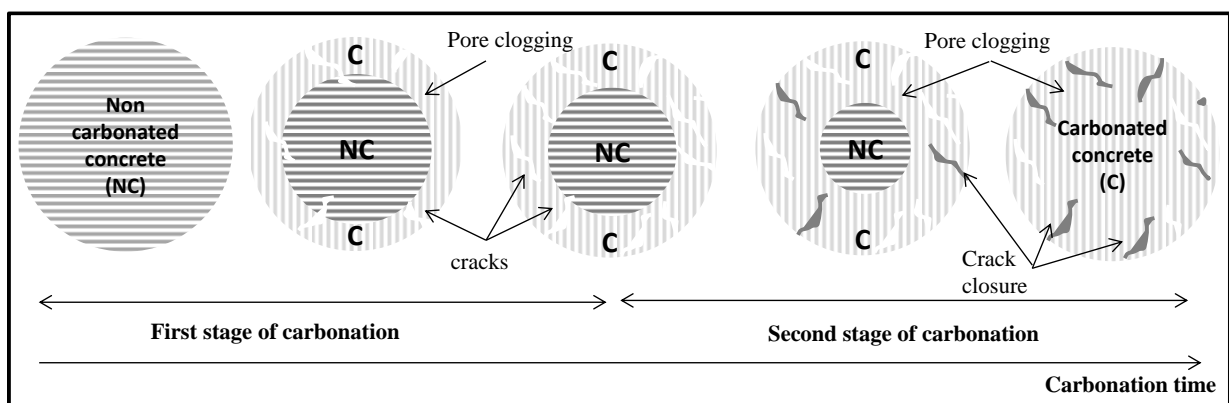
550

551 **Figure 17 : Evolution of permeability during carbonation**

552 The evolution of permeability with CSP is mostly similar for the three curves considered in
553 this study with a slight shift of the maximum towards lower CSP with specimens drying. An
554 increase in the gas permeability could be observed at the initial stage of carbonation although
555 the total porosity continuously decreased (Figure 15). Such increase has also been observed
556 by Pham et al in 2013 [46] and Thiery in 2005 [26]. The carbonation shrinkage, the tensile
557 stresses and the increase in hardness makes the carbonated zone more prone to cracking [28]
558 [53]. These cracks and microcracks could contribute to the development of macropores as

559 pointed out by mercury intrusion porosimetry, and together they explain the increase in gas
560 permeability obtained in this first stage of carbonation [26] [46].

561 Then, as the carbonation progressed, the permeability decreased. This change observed in the
562 evolution of permeability (increases then decreases) is original. The observed decrease in
563 permeability shows the dominant effect of pore-clogging and decrease in porosity. This step
564 began when a significant part of the surface was carbonated. At this stage the carbonation
565 shrinkage has started to stabilize and the gradients of properties across the different zones
566 attenuates leading to the reduction of the tensile stresses. At the same time the clogging of the
567 pores and the closure of microcracks continue. ~~In this case the clogging not only reduces the~~
568 ~~volume of the pores but at the same time ensures ensuring the healing of microcracks already~~
569 ~~present or developed during carbonation. In addition, carbonation shrinkage of the inner zone~~
570 ~~of the cross section causes the closure of cracks developed in the outer zone and thus the~~
571 ~~closing of the macropores as observed after 100 days of carbonation in previous section. This~~
572 ~~induces and consequently induce~~ a decrease in the permeability of the material. Figure 18
573 summarizes the different mechanisms that take place during the two identified stages of
574 carbonation.



575

576

Figure 18 : Schematic drawing of the different stages of carbonation

577 4 Conclusion

578 The adhesive old mortar on recycled concrete aggregates seriously affects their properties and
579 therefore the behavior of recycled aggregate concrete. Revealing the variation in the
580 microstructure and transport properties of cement mortars subjected to an accelerated
581 carbonation treatment through a multiscale investigation allows understanding the effects of
582 carbonation on recycled aggregates made with cement-based materials and consequently on
583 the behavior and durability of resulting concrete. From the experimental results and
584 discussion above, the following conclusions can be drawn:

- 585 • During the first stage, the carbonation of portlandite dominates leading, in a basic
586 medium, to the precipitation of calcite which is the stable polymorph of calcium
587 carbonate. As the carbonation progresses the portlandite is depleted, and therefore the
588 pH of the concrete decreases, the carbonation of C-S-H begins to prevail leading to the
589 precipitation of unstable polymorphs of CaCO_3 (aragonite and vaterite). ~~such as~~
590 ~~vaterite.~~
- 591 • The ~~variations of porosity and~~ evolution of mechanical properties during carbonation
592 depends on the nature of the precipitated polymorph of calcium carbonate. ~~The~~
593 ~~formation of vaterite during the last stage of carbonation results in a significant~~
594 ~~increase of elastic modulus both at local and macroscopic scales.~~
- 595 • ~~The carbonation shrinkage developed during accelerated carbonation is significant.~~
596 ~~Carbonation shrinkage and tensile stresses developed during accelerated carbonation~~
597 ~~are likely to cause significant damage and cracking, as evidenced by permeability~~
598 ~~data.~~
- 599 • Two main stages are present at the material scale. During the first phase, contradictory
600 mechanisms develop in the cement paste: clogging of the pores and cracking. The
601 experimental data show that the effects of these two mechanisms nearly compensate in

602 terms of macroscopic elastic modulus but they induce an increase in permeability at
603 the start of carbonation.

- 604 • The second stage begins when most of the surface is carbonated. At this stage, pore
605 clogging and microcracks closing dominates cracking. This explains the improvement
606 observed in the elastic modulus and the continuous reduction in the total porosity
607 accessible to water and permeability of the material.

608 **Acknowledgements**

609 The financial support from Ecole Centrale de Nantes through the PhD thesis grant of Mrs
610 Farah Kaddah is gratefully acknowledged.

611 **References**

- 612 [1] C.-S. Poon and D. Chan, “The use of recycled aggregate in concrete in Hong Kong,”
613 Resources, Conservation and Recycling, p. 13, 2007.
- 614 [2] C. Liang, N. Lu, H. Ma, Z. Ma, and Z. Duan, “Carbonation behavior of recycled concrete
615 with CO₂-curing recycled aggregate under various environments,” Journal of CO₂
616 Utilization., p. 101185, Jul. 2020.
- 617 [3] D. Kong, T. Lei, J. Zheng, C. Ma, J. Jiang, and J. Jiang, “Effect and mechanism of
618 surface-coating pozzalanic materials around aggregate on properties and ITZ
619 microstructure of recycled aggregate concrete,” Construction and Building Materials, p. 8,
620 2010.
- 621 [4] P. Belin, G. Habert, M. Thiery, and N. Roussel, “Cement paste content and water
622 absorption of recycled concrete coarse aggregates,” Materials and Structures, pp. 1451–
623 1465, Sep. 2014.
- 624 [5] D. Xuan, “Assessment of mechanical properties of concrete incorporating carbonated
625 recycled concrete aggregates,” Cement and Concrete Composites, p. 8, 2016.
- 626 [6] A. Z. Bendimerad, E. Roziere, and A. Loukili, “Combined experimental methods to
627 assess absorption rate of natural and recycled aggregates,” Materials and Structures, pp.
628 3557–3569, Nov. 2015.
- 629 [7] K. McNeil and T. H.-K. Kang, “Recycled Concrete Aggregates: A Review,” International
630 Journal of Concrete Structures and Materials, pp. 61–69, Mar. 2013
- 631 [8] J. Zhang, C. Shi, Y. Li, X. Pan, C.-S. Poon, and Z. Xie, “Influence of carbonated recycled
632 concrete aggregate on properties of cement mortar,” Construction and Building Materials,
633 pp. 1–7, Nov. 2015.
- 634 [9] C. S. Poon, Z. H. Shui, and L. Lam, “Effect of microstructure of ITZ on compressive
635 strength of concrete prepared with recycled aggregates,” Construction and Building
636 Materials., pp. 461–468, Jul. 2004.

- 637 [10] N. Lippiatt, T.-C. Ling, and S.-Y. Pan, "Towards carbon-neutral construction
638 materials: Carbonation of cement-based materials and the future perspective," *Journal of*
639 *Building Engineering*, p. 101062, Mar. 2020.
- 640 [11] J. Pacheco and J. de Brito, "Recycled aggregates produced from construction and
641 demolition waste for structural concrete: constituents, properties and production,"
642 *Materials*, p. 5748, Oct. 2021.
- 643 [12] R. V. Silva, J. de Brito, and R. K. Dhir, "Use of recycled aggregates arising from
644 construction and demolition waste in new construction applications," *Journal of Cleaner*
645 *Production*, p. 117629, Nov. 2019.
- 646 [13] S. Jayakody, A. M. Z. Zimar, and R. A. L. M. Ranaweera, "Potential use of recycled
647 construction and demolition waste aggregates for non- structural concrete applications"
648 *Journal of the National Science Foundation of Sri Lanka* p. 205, Jun. 2018.
- 649 [14] V. W. Y. Tam, C. M. Tam, and K. N. Le, "Removal of cement mortar remains from
650 recycled aggregate using pre-soaking approaches," *Resources, Conservation and*
651 *Recycling*, pp. 82–101, Mar. 2007.
- 652 [15] B. Zhan, C. S. Poon, Q. Liu, S. Kou, and C. Shi, "Experimental study on CO₂ curing
653 for enhancement of recycled aggregate properties," *Construction and Building Materials*,
654 pp. 3–7, Sep. 2014.
- 655 [16] S.-C. Kou, B. Zhan, and C.-S. Poon, "Use of a CO₂ curing step to improve the
656 properties of concrete prepared with recycled aggregates," *Cement and Concrete*
657 *Composites*, pp. 22–28, Jan. 2014.
- 658 [17] S. K. Kaliyavaradhan, T.-C. Ling, and K. H. Mo, "CO₂ sequestration of fresh concrete
659 slurry waste: Optimization of CO₂ uptake and feasible use as a potential cement binder"
660 *Journal of CO₂ Utilization*, p. 101330, Dec. 2020.
- 661 [18] J. Zhan, "Carbonation treatment of recycled concrete aggregate_ Effect on transport
662 properties and steel corrosion of recycled aggregate concrete," *Cement and Concrete*
663 *Composites*, p. 8, 2019.
- 664 [19] Y. F. Houst and F. H. Wittmann, "Retrait de carbonatation," *Ein Dienst der ETH-*
665 *Bibliothek*, p. 255, 1989.
- 666 [20] C. Pade and M. Guimaraes, "The CO₂ uptake of concrete in a 100 year perspective,"
667 *Cement and Concrete Research.*, p. 9, 2007.
- 668 [21] M. Sereng, "Improvement of the properties of recycled aggregates by CO₂ storage:
669 pre-industrial feasibility study," *University of Paris-Est, France, 2020, PhD thesis.*
- 670 [22] J. Zhang, C. Shi, Y. Li, X. Pan, C.-S. Poon, and Z. Xie, "Performance enhancement of
671 recycled concrete aggregates through carbonation," *Journal of Materials in Civil*
672 *engineering*, p. 04015029, Nov. 2015.
- 673 [23] D. Wang, T. Noguchi, and T. Nozaki, "Increasing efficiency of carbon dioxide
674 sequestration through high temperature carbonation of cement-based materials," *Journal*
675 *of Cleaner Production*, p. 117980, Nov. 2019.
- 676 [24] G. Pan, M. Zhan, M. Fu , Y. Wang, X. Lu "Effect of CO₂ curing on demolition
677 recycled fine aggregates enhanced by calcium hydroxide pre-soaking," *Construction and*
678 *Building Materials*, p. 9, 2017.
- 679 [25] Y. F. Houst, "The role of moisture in the carbonation of cementitious materials,"
680 *Internationale Zeitschrift für*, p. 18, 1996.
- 681 [26] M. Thiery, " Modeling of atmospheric carbonation of cementitious materials:
682 Consideration of kinetic effects and microstructural and water modifications" *Ecole*
683 *nationale des ponts et chaussées, France, 2007, PhD thesis*
- 684 [27] J. Han, W. Sun, G. Pan, and W. Caihui, "Monitoring the evolution of accelerated
685 carbonation of hardened cement pastes by X-Ray computed tomography," *Journal of*
686 *Materials in Civil Engineering*, pp. 347–354, 2013.

- 687 [28] D. Cui, X. Zuo, K. Zheng, and S. Talukdar, "Tomography-based investigation on the
688 carbonation behavior through the surface-opening cracks of sliced paste specimen"
689 materials, p. 17, 2020.
- 690 [29] E. Drouet, "Impact of temperature on the carbonation of cementitious materials:
691 consideration of water transfers" Ecole normale supérieure de Cachan, France, 2011, PhD
692 thesis.
- 693 [30] R. E. Hachem, "Multicriteria study of the degradation of cementitious materials by
694 external sulphate attack" Ecole Centrale de Nantes, France, 2010, PhD thesis.
- 695 [32] M. Khachani, A. E. Hamidi, M. Halim, and S. Arsalane, "Non-isothermal kinetic and
696 thermodynamic studies of the dehydroxylation process of synthetic calcium hydroxide
697 Ca(OH)₂," Journal of Materials and Environmental Science, p. 11, 2014.
- 698 [33] G. Villain, M. Thiery, and G. Platret, "Measurement methods of carbonation profiles
699 in concrete: Thermogravimetry, chemical analysis and gammadensimetry," Cement and
700 Concrete Research, pp. 1182–1192, Aug. 2007.
- 701 [34] A. Morandeau, "Investigation of the carbonation mechanism of CH and C-S-H in
702 terms of kinetics, microstructure changes and moisture properties," Cement and Concrete
703 Research, p. 18, 2014.
- 704 [35] E. Rozière, A. Loukili, and F. Cussigh, "A performance based approach for durability
705 of concrete exposed to carbonation," Construction and Building Materials ,pp. 190–199,
706 Jan. 2009.
- 707 [36] G. S. dos Reis, B. G. Cazacliu, R. Artoni, and J. Torrenti, "Effect of the accelerated
708 carbonation treatment on the recycled sand physicochemical characteristics through the
709 rolling carbonation process," Journal of CO₂ Utilization., p. 101181, Jul. 2020.
- 710 [37] Y. Pu, L. Li, Q. Wang, X. Shi, L. Fu, G. Zhang, C. Luan, A. Abomohra, "Accelerated
711 carbonation treatment of recycled concrete aggregates using flue gas: A comparative
712 study towards performance improvement," Journal of CO₂ Utilization, p. 101362, Jan.
713 2021.
- 714 [38] Y. Li et al., "Carbonation of the synthetic calcium silicate hydrate (C-S-H) under
715 different concentrations of CO₂: Chemical phases analysis and kinetics," Journal of CO₂
716 Utilization., pp. 303–313, Jan. 2020.
- 717 [39] J. Grandet, "Contribution to the study of the setting and carbonation of mortars in
718 contact with porous materials " Universiy of Paul Sabatier Toulouse, France, 1975, PhD
719 thesis
- 720 [40] J. Chang, D. Wang, and Y. Fang, "Effects of mineralogical changes in BOFS during
721 carbonation on pH and Ca and Si leaching," Construction and Building Materials, pp.
722 584–592, Dec. 2018.
- 723 [41] Ç. Oral, "Influence of pH on morphology, size and polymorph of room temperature
724 synthesized calcium carbonate particles," Powder Technology., p. 8, 2018.
- 725 [42] B. Kammoe and R. Brice, "Synthèse de nanoparticules de carbonate de calcium," p.
726 92.
- 727 [43] R. Sevik, "Physical and nanomechanical properties of the synthetic anhydrous
728 crystalline CaCO₃ polymorphs: vaterite, aragonite and calcite", J Mater Sci, 2018.
- 729 [44] H. Nebel and M. Epple, "Continuous preparation of calcite, aragonite and vaterite, and
730 of magnesium-substituted amorphous calcium carbonate (Mg-ACC)," Z. Für Anorg. Allg.
731 Chem., pp. 1439–1443, Jul. 2008.
- 732 [45] D. Xuan, B. Zhan, and C. S. Poon, "Assessment of mechanical properties of concrete
733 incorporating carbonated recycled concrete aggregates," Cement and Concrete
734 Composites, pp. 67–74, Jan. 2016.

- 735 [46] S. T. Pham, “Modifications on microporosity and physical properties of cement mortar
736 caused by carbonation: comparison of experimental methods,” Hindawi Publishing
737 Corporation, p. 10, 2013.
- 738 [47] M. Auroy, “Impact of carbonation on unsaturated water transport properties of
739 cement-based materials” *Cement and Concrete Research*, p. 288, 2015.
- 740 [48] N. Hyvert, “Application of the probabilistic approach to the durability of precast
741 concrete products” *University of Toulouse, France, 2009 PhD thesis*.
- 742 [49] S. T. Pham, “Modifications in water sorption isotherms of cement mortars caused by
743 carbonation: effects of cycles,” *Advanced Materials Research*., pp. 3–9, Oct. 2014.
- 744 [50] H. Jiande, S. Wei, P. Ganghua, W. Caihui, and R. Hui, “Application of X-ray
745 computed tomography in characterization microstructure changes of cement pastes in
746 carbonation process,” *Journal of Wuhan University of Technology-Mater Sci Ed*, p. 7,
747 April 2012.
- 748 [51] J. J. Chen, J. J. Thomas, and H. M. Jennings, “Decalcification shrinkage of cement
749 paste,” *Cement and Concrete Research*, pp. 801–809, May 2006.
- 750 [52] E. Kangni-Foli, S. Poyet, P. Le Bescop, T. Charpentier, F. Bernachy-Barbé, A.
751 Dauzères, E. L’Hopital a, J.-B. d’Espinose de Lacaillerie, “Carbonation of model cement
752 pastes: The mineralogical origin of microstructural changes and shrinkage,” *Cement and
753 Concrete Research*., p. 106446, Jun. 2021.
- 754 [53] H. Jiande, S. Wei, P. Ganghua, W. Caihui, and R. Hui, “Application of X-ray
755 Computed Tomography in characterization microstructure changes of cement pastes in
756 carbonation process,” *Journal of Wuhan University of Technology-Mater Sci Ed*, p. 7,
757 April 2012.
- 758 [54] C.-F. Chang, “Strength and elastic modulus of carbonated concrete.”, *ACI materials
759 journal*, 2005
- 760 [55] C. A. Garcia-Gonzalez, A. Hidalgo, C. Andrade, M. Cruz Alonso, J. Fraile, A. M.
761 Lopez-Periago, and C. n Domingo, “Modification of composition and microstructure of
762 portland cement pastes as a result of natural and supercritical carbonation procedures,”
763 *Industrial & Engineering Chemistry Research*, p. 8, 2006.
- 764 [56] A. Younsi, “Carbonation of concretes with high rates of substitution of cement by
765 mineral additions,” *University of La Rochelle, France, 2012, PhD thesis*.
- 766 [57] T. Danner and M. R. Geiker, “Long-term Influence of concrete surface and crack
767 orientation on self-healing and ingress in cracks – Field Observations,” *Nordic Concrete
768 Research*, pp. 1–16, Jun. 2018.
- 769 [58] Carola Edvardsen, “Water permeability and autogenous healing of cracks in concrete,”
770 *ACI materials journal*, Jan. 1999.
- 771 [59] B. A. Silva, A. P. Ferreira Pinto, A. Gomes, and A. Candeias, “Effects of natural and
772 accelerated carbonation on the properties of lime-based materials,” *Journal of CO₂
773 Utilization*.,p. 101552, Jul. 2021.
- 774 [60] V. T. Ngala and C. L. Page, “Effects of carbonation on pore structure and diffusional
775 properties of hydrated cement pastes” *Cement and Concrete Research*., pp. 995–1007, Jul.
776 1997.
- 777 [61] T. A. Bier, “Influence of type of cement and curing on carbonation progress and pore
778 structure of hydrated cement pastes,” 1987.